THE FAILURE MECHANISM OF A NICKEL ELECTRODE IN A NICKEL-HYDROGEN CELL*

H.S. Lim and S.A. Verzwyvelt

Hughes Research Laboratories

ABSTRACT

Studies on a number of types of nickel electrodes after cycle failure in a Ni/H_2 cell showed that the failure is due to the loss of high rate discharge capability rather than an absolute capacity loss. The failure mechanism is speculated to be a combination of migration of the active material away from the current collecting nickel sinter, increased porosity of the active material caused by cycling, and an electrical isolation process of the active material during discharge.

INTRODUCTION

Nickel-hydrogen cells are used for spacecraft energy storage systems which require a long cycle life and low weight batteries. The useful weight and cycle life of the cell are closely related to each other. When the depth-of-discharge (DOD) of the cell operation is increased, the effective cell weight is decreased in an inversely proportional manner; however, the cycle life will also decrease. The cycle life and the weight of a Ni/H_2 cell can be exchanged for a lighter weight if necessary.

Nickel electrodes have been recognized as key life-limiting components of the Ni/H_2 cell. Therefore, understanding the failure mechanism of the nickel electrode is of paramount importance for understanding the limitations of the Ni/H_2 cell and for further improvements of the cell.

NICKEL ELECTRODE TYPES AND TEST CELLS

All electrodes used in this study were sinter type of various designs. The details of electrode types and test cells have been described elsewhere (Ref. 1-3), except for those electrodes used for BET surface area and the sinter damage studies. The electrode samples for these studies were typical flight quality nickel electrodes for Ni/H_2 cells of the standard Hughes/USAF design. These electrodes were evaluated before and after a 6400 cycle life test at 80% DOD in a Ni/H_2 cell.

CHANGES OF ELECTRODE CAPACITY AND RATE DEPENDENCE DURING CYCLE LIFE TEST

The change in nickel electrode capacity by cycling is shown in Figure 1 in terms of the active material utilization. The utilization is defined as

*This work was partially supported by NASA-Lewis Research Center under Contract No. NAS 3-22238 (Contract Manager, John Smithrick).

the ratio of the measured capacity to the theoretical capacity which represents the total amount of the active material in the electrode. The capacity or utilization decreased gradually as the electrode was cycled. Capacities of a Ni/H_2 cell before and after a 12960 cycle test are shown in Figure 2 as a function of discharge rates. The capacity of the cell was limited by the nickel electrodes.

The capacity depended on the discharge rate showing decreased capacity at an increased rate. The average difference in the initial capacities of 19 cells between the discharge rates of 2.74C and 0.5C was 3.3%. After the cycle life test this dependence increased markedly, in addition to the overall capacity decrease, as shown in Figure 2. The cell capacity decreased sharply as the discharge rate increased. The average capacity at the discharge rate of 2.74C was 19% less than at the 0.5C rate. At a very low discharge rate (C/10 rate) the cell capacity after the cycle test approached its initial value, indicating that the absolute cell capacity did not decrease significantly. These results also indicate that the cycling failure of a Ni/H_2 cell is due to this loss of high rate discharge capability in nickel electrodes rather than an absolute loss of the electrode capacity. In summary, these results indicate that the electrode degradation involves a gradual loss of the high rate discharge capability as the electrode is aged by cycling.

CHANGES OF NICKEL ELECTRODES AFTER CYCLE LIFE TESTS

Many changes of nickel electrodes have been observed after a cycle life test of various Ni/H_2 cells. These changes include dimensional (thickness) expansion, rupture of sinter structure, loose black powder formation, increase of BET surface area, change of pore distribution, increase of pore volume, and active material migration as described below.

The thickness of the electrode expands as the electrode is cycled. The degree and the rate of the expansion depend strongly on the level of the active material loading in the electrode, as shown in Figure 3. This electrode expansion often accompanies the rupture of the substrate sinter structure, as shown in Figure 4. Loose black powder of the active material was observed on the surface of nickel electrodes and other cell components adjacent to the electrode in cycled cells. The powder on the gas screen and back side of a hydrogen electrode from a cycled cell is shown in Figure 5.

The BET surface area of a nickel electrode increased after cycling. The increase of the surface area appears to be mainly in the pore range of 50 to 100 Å, as shown in Figure 6. Direct measurements of the pore distribution using a mercury intrusion porosimetry also showed a large increase of pores in the same pore radius range, as shown in Figure 7. These increases in pore volume and surface area indicate that the active material expands with the formation of additional pores in the range of 50 to 100 Å as the electrode is cycled.

The expansion of active material inside the porous sinter structure inevitably leads to active material migration, as shown in Figures 8 and 9. The light dots and the large circular area in the picture are nickel sinter

and nickel wire mesh substrate, respectively. The grey area represents the active material. New electrodes have a relatively uniform pore structure of sinter in which the active material is impregnated. Because of this uniformity, the active material in the new electrode is distributed more closely (roughly within 10 μm) to the current collecting nickel sinter particles. In cycled electrodes, however, the distritution of the active material is no longer uniform due to the migration of the active material. The change is readily noticeable, regardless of the active material loading level, sinter structure, or degree of the electrode expansion (Figures 8 and 9). All of the changes discussed above were apparently the result of irreversible active material expansion which occurred during cycling (Ref. 4). As the active material expanded inside the pores of the nickel sinter, a portion of the active material was extruded out of the pores to the outside of the sinter or into void pockets of the sinter. This extrusion appeared to occur without sinter damage in a large pore (16 μm) sinter such as 2540 type plaque (Ref. 1). However, when there was an insufficient amount of void volume (e.g., in heavily loaded electrodes) and the extrusion was restricted by small pores of the plaque, the active material expansion fractured the sinter structure, often into layers along the plane of the electrode, as shown in Figures 4 and 8. Regardless of whether the sinter was ruptured or not, the extrusion of the active material resulted in a migration in which a significant portion of the active material moved away from the vicinity of the current collecting sinter.

FAILURE MECHANISM OF NICKEL ELECTRODES

Although several physical changes have been observed, as discussed above, only two of these are apparently related to the failure of the nickel electrode at the high rate cycling of a low earth orbit regime. These two are the active material migration away from the current collecting nickel sinter particles and the density reduction of active material by the increase of the pore volume in the pore radius range of 50 to 100 Å.

Other changes such as the dimensional expansion and the rupture of the sinter structure were not observed with every failed electrode, indicating that these changes are not a necessary condition of the failure. In addition, some failed electrodes with severe expansion and sinter rupture cycled much longer than those without such changes. The formation of black powder in varying degrees, was observed in all failed electrodes. However, the amount of the black powder material was estimated to be fairly minor portion of the active material. In addition, the capacities of some failed electrodes were close to the initial capacity when measured at a very low discharge rate (Figure 2), indicating that the capacity loss due to the black powdering is relatively small. An increase of the BET surface area was also observed with all the failed electrodes. However, the magnitude of the increase varied depending on the number of cycles to the failure, lacking a consistent value for the failure.

The active material migration away from the current collector and the pore volume increase (density reduction) of the active material were observed with every failed electrode. It appears that the failure mechanism has to be

closely related to these two changes. An explanation of the capacity decrease at the high rate discharge has been speculated to be a combination of an electrical isolation mechanism of charged active material during discharge (Ref. 5-7) and the presently observed migration and density reduction of the active material. The mechanism of the charge propagation through the active material may be complex (Ref. 6-7), especially in view of the porous nature of the active material. For example, no information is available on the polarization of electrolyte in the micropores of the active material and the tortuosity of the pore structure. However, a rough model is offered below to explain the capacity reduction, assuming that the polarization of the electrolyte in the micropores is not the major factor in the propagation of the discharge reaction.

In a new electrode the active material is relatively uniformly distributed in the vicinity (roughly within 10 μm) of the current collecting nickel sinter, as illustrated schematically in Figure 10(a) and 10(b). In an electrode cycled to failure, however, a significant portion of the active material has moved away from the sinter, as shown schematically in Figure 10(c) and 10(d). When a new electrode is charged and discharged the active material is more or less fully and uniformly utilized. In a cycled electrode, as shown in Figure 10(c) and 10(d), however, the active material is expected to be fully charged, but a portion of the active material may not be fully discharged (Figure 10(d)). This is because the active material in the charge state is a good conductor (Ref. 8) while the one in the discharged state is a poor conductor (Ref. 6). The active material in the vicinity of the current collector may be discharged before the portion away from the current collector has a chance to be fully discharged because of the potential drop accross the porous active material. When this occurs the undischarged active material will be electrically isolated from the current collector.

The electrical isolation process of the charged active material is expected to depend on the discharge rate. The anticipated discharge rate effect of a microscopic area of the electrode (Figure 11) is illustrated in Figure 12. As the active material becomes more porous by cycling, the electrical isolation process will occur more readily becuase the overall conductivity of the material will be reduced progressively. Although we do not fully understand the pressure behavior of Ni/H_2 cells during cycle tests (Ref. 2), this overall scheme of the speculated failure mechanism of the nickel electrode appears to be consistent with the physical changes of the electrode after cycling.

REFERENCES

1. H.S. Lim and S.A. Verzwvelt, "Long Life Nickel Electrodes For a Nickel-Hydrogen Cell: III. Results of an Accelerated Test and Failure Analyses," Proc. 19th Intersociety Energy Conversion Engineering Conference, August 1984, p. 312.

2. H.S. Lim and S.A. Verzwyvelt, "Long Life Nickel Electrodes For a Nickel-Hydorgen Cell: Cycle Life Tests," Proc. 31st Power Sources Symposium, Cherry Hill, N.J. June, 1984.

3. H.S. Lim, S.A. Verzwyvelt, C. Bleser, and K.M. Keener, "Long Life Nickel Electrodes For a Nickel-Hydorgen Cell: I. Initial Performance," Proc. 18th Intersociety Energy Conversion Engineering Conference, August 1983, p. 1543.

4. H.S. Lim and S.A. Verzwvelt, "Expansion Mechanisms of the Nickel Electrode in an Alkaline Storage Cell: I. Electrode Bending Experiments," Proc. 15th Intersociety Energy Conversion Engineering Conference, Aug. 1980, p. 1619.

5. C.K. Dyer, "Chargeability of Ni Electrodes Studied by Optical Microscopy," The Nickel Electrode, ed. by R.G. Gunther and S. Gross (The Electrochemical Society, Pennington, N.J. 1982), Proceeding Vol. 82-4, p. 118.

6. R. Barnard, G.T. Crickmore, J.A. Lee and F.L. Tye, J. Appl. Electrochem., 10, 61 (1980).

7. R. Barnard, C.F. Randell and F.L. Tye, J. Appl. Electrochem., 10, 109 (1980).

8. D. Tuomi and G.J.B. Crawford, J. Electrochem. Soc., 115, 450 (1968).

FIGURE CAPTIONS

1. Active material utilization of various nickel electrodes as a function of number of cycles. Electrode types: A; 8740M, B; 8770M, C; 8755M, D; 5540M, E; 5555M, and F; 5570M. The utilization was measured by discharging Ni/H_2 cells to 1.0 V at 1.37C rate after charging for 80 min. at C rate.

2. Capacities of a Ni/H_2 cell (BP13 of Ref 1) at various discharge rates before and after a cycle life test.

3. Nickel electrode expansion as a function of the number of 80% depth-of-discharge cycles. Active material loading level of the electrode is indicated by various symbols.

4. Cross sectional view of nickel sinter substrate of a new nickel electrode (A) and a similar electrode after 6400 cycles. The samples were prepared after the active material was dissolved out.

5. Photograph of the gas screen and back side of the hydrogen electrode from a cycled Ni/H_2 cell.

6. Change of BET surface area of a nickel electrode by cycling.

7. Cumulative pore volume distribution of various new and cycled nickel electrodes by a mercury intrusion porosimetry.

8. SEM cross sectional view of new (A) and cycled (B) (12,960 cycles) nickel electrodes (8740M) with 1.52 g/cc void of active material loading.

9. SEM cross sectional view of new (A and C) and cycled (B: 2330 cycles and D: 2340 cycles) nickel electrodes of various types. (A) and (B): 2540L type; 1.37 g/cc void loading. (C) and (D): 2540H type; 1.64 g/cc void loading.

10. A schematic illustration of nickel electrode capacity decrease.

11. A schematic representation of a microscopic portion of a nickel electrode.

12. A schematic illustration of discharge rate dependence of electrode capacity.

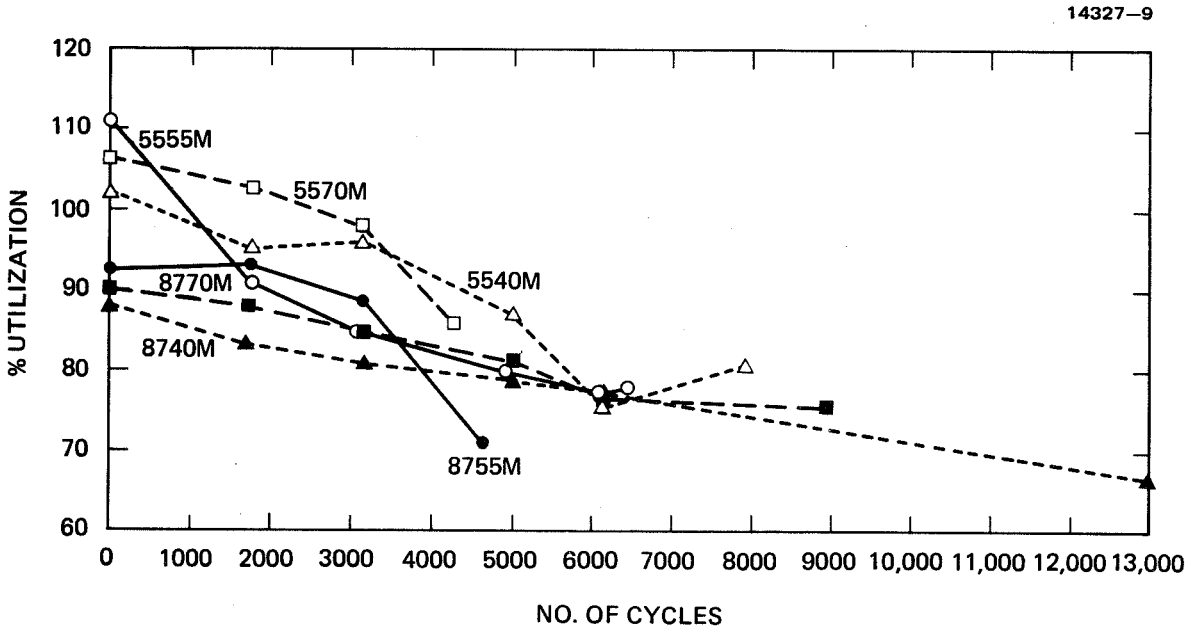

Figure 1. Active material utilization of various nickel electrodes as a function of number of cycles. Electrode types: A, 8740M; B, 8770M; C, 8755M; D, 5540M; E, 5555M; and F, 5570M. The utilization was measured by discharging Ni/H_2 cells to 1.0V at 1.37C rate after charging for 80 min. at C rate.

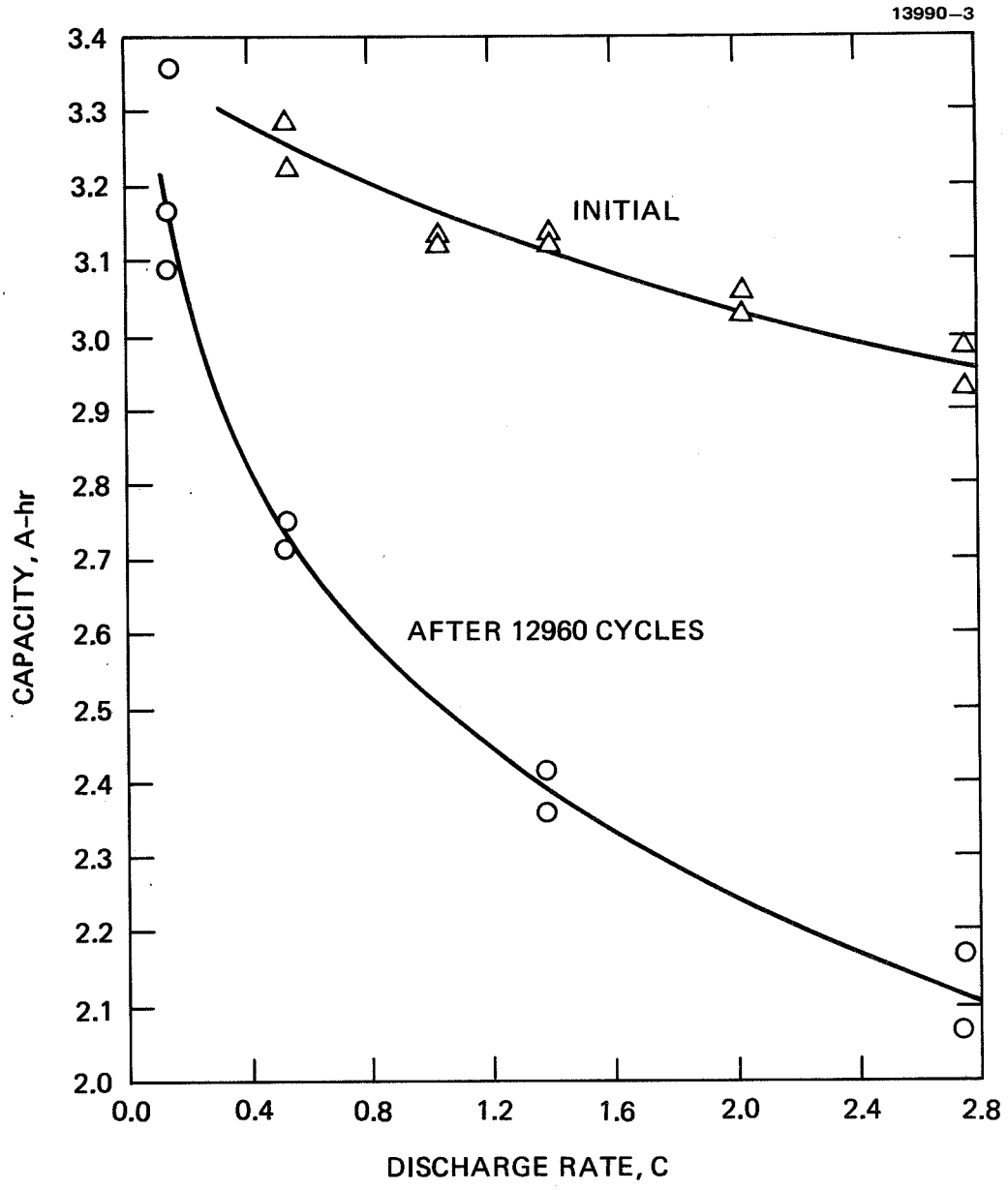

Figure 2. Capacities of a Ni/H_2 cell (BP13 of Ref. 1) at various discharge rates before and after a cycle life test.

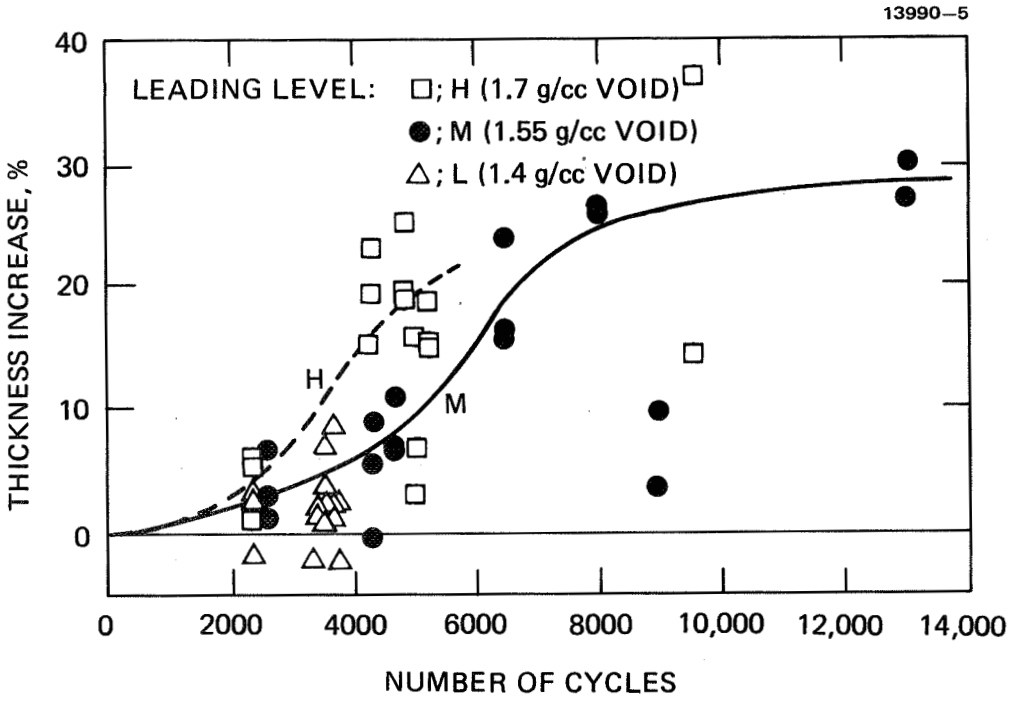

Figure 3. Nickel electrode expansion as a function of the number of 80% depth-of-discharge cycles. Active material loading level of the electrode is indicated by various symbols.

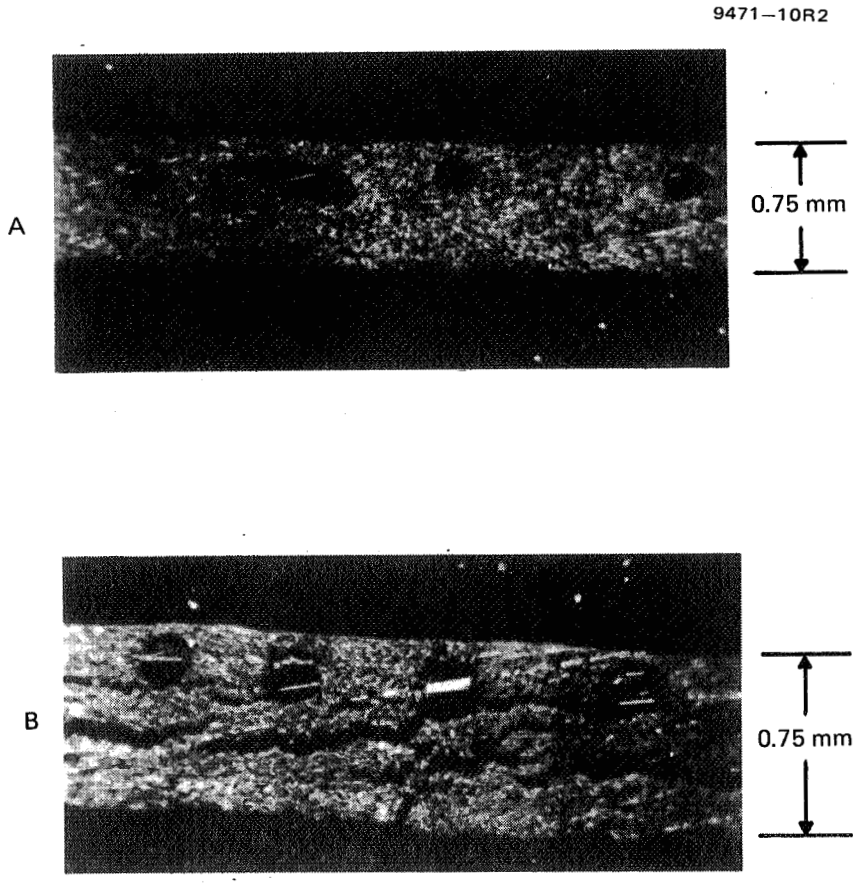

Figure 4. Cross sectional view of nickel sinter substrate of a new nickel electrode (A) and a similar electrode after 6400 cycles. The samples were prepared after the active material was dissolved out.

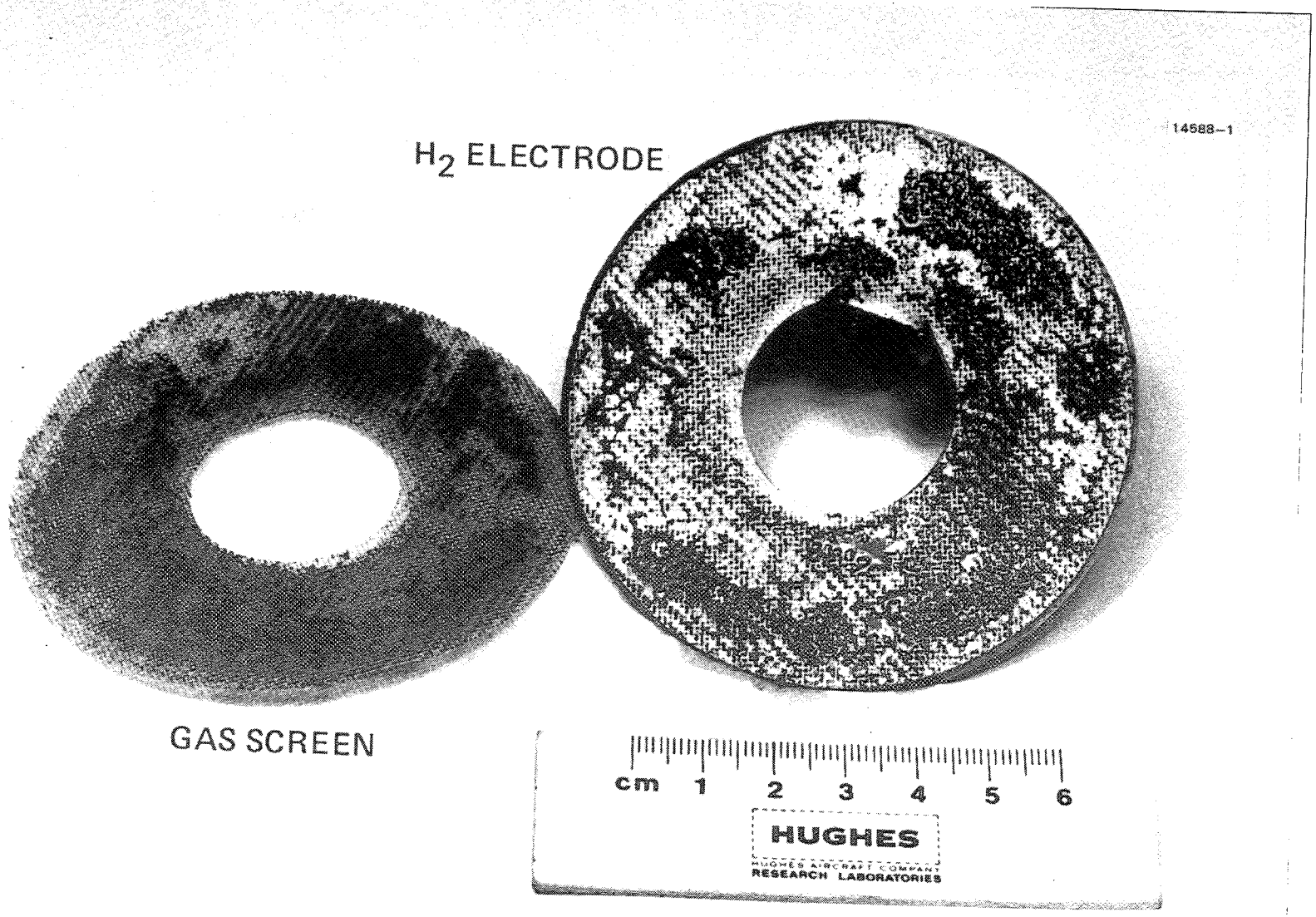

Figure 5. Photograph of the gas screen and back side of the hydrogen electrode from a cycled Ni/H_2 cell.

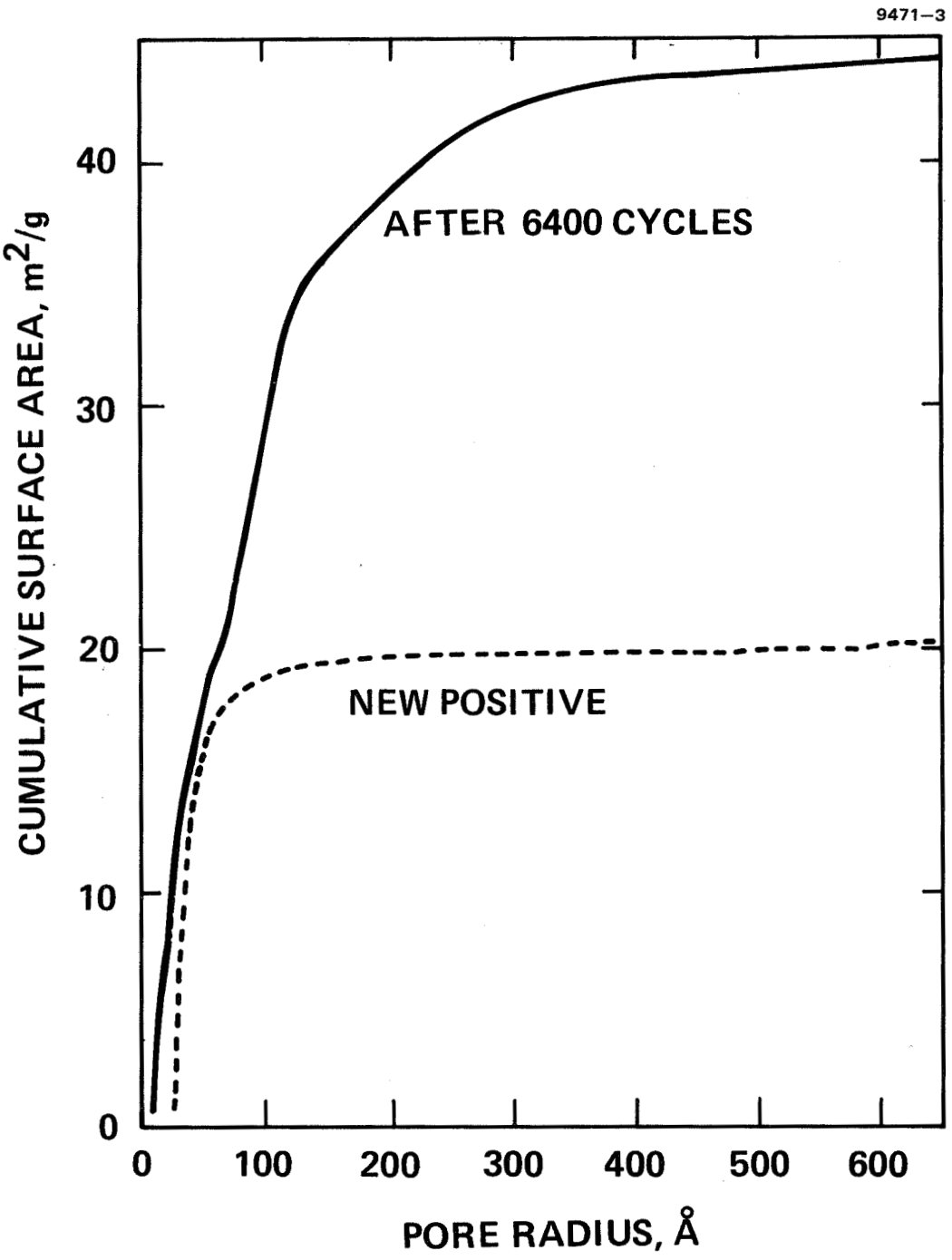

Figure 6. Change of BET surface area of a nickel electrode by cycling.

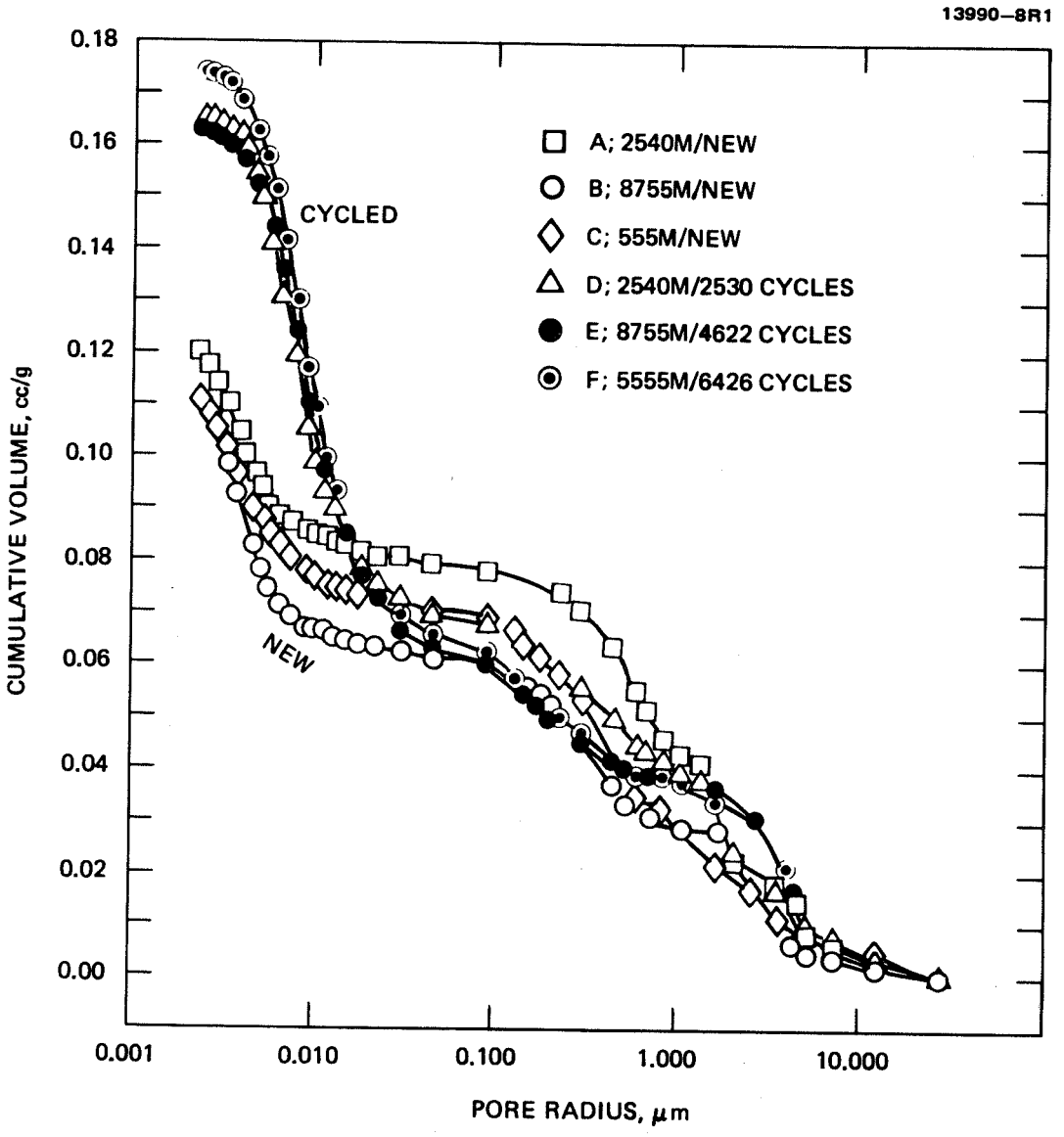

Figure 7. Cumulative pore volume distribution of various new and cycled nickel electrodes by a mercury intrusion porosimetry.

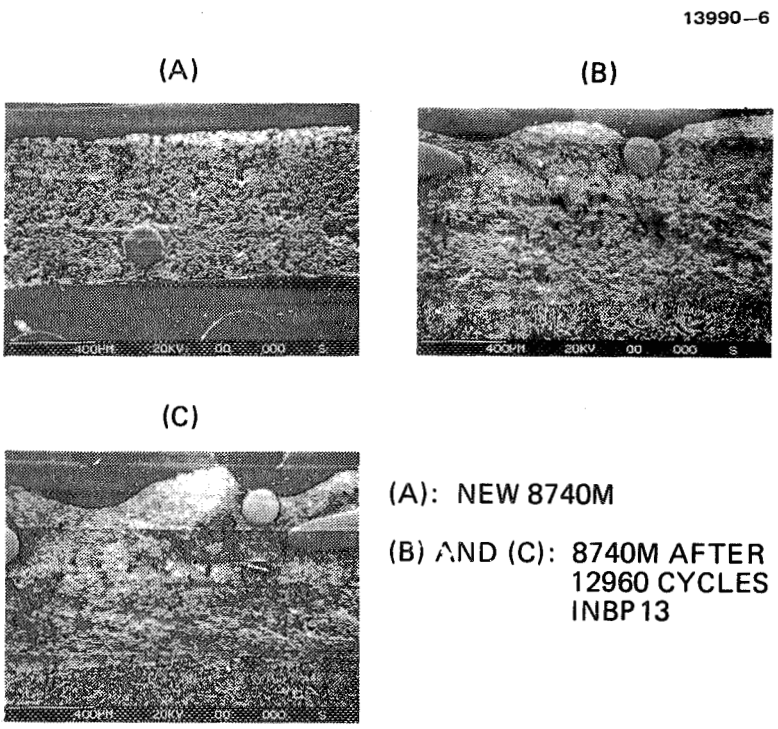

Figure 8. SEM cross sectional view of new (A) and cycled (B) (12,960 cycles) nickel electrodes (8740M) with 1.52 g/cc void of active material loading.

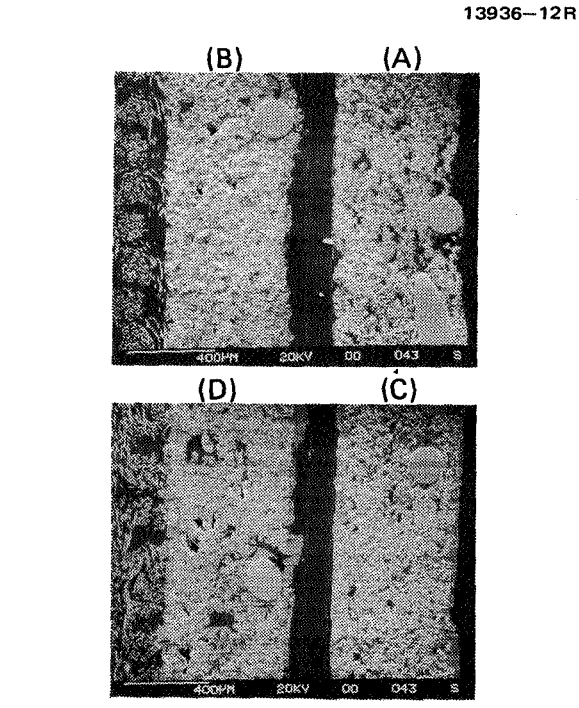

Figure 9. SEM cross sectional view of new (A and C) and cycled (B: 2330 cycles and D: 2340 cycles) nickel electrodes of various types. (A) and (B): 2540L type; 1.37 g/cc void loading. (C) and (D): 2540H type; 1.64 g/cc void loading.

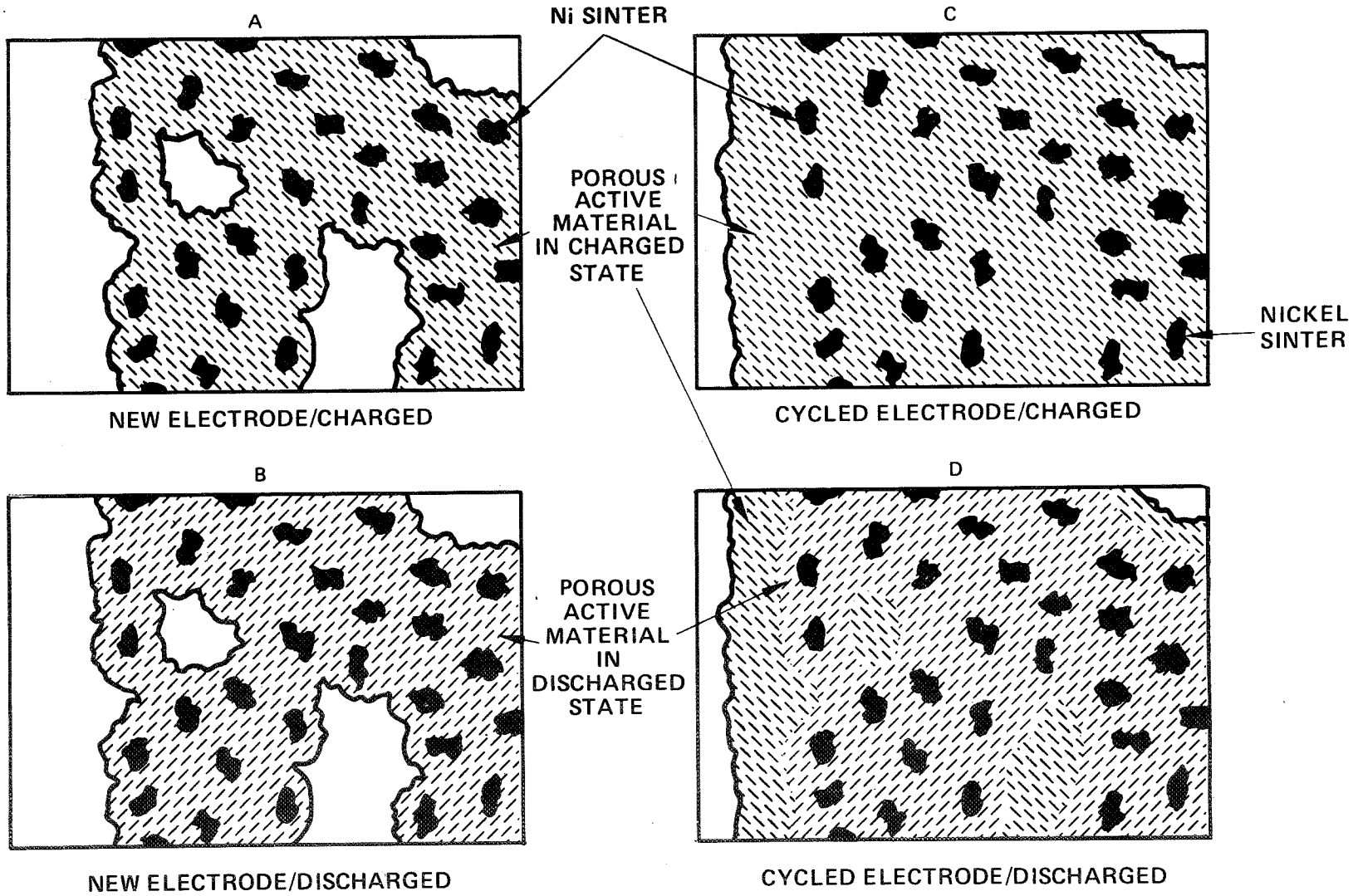

Figure 10. A schematic illustration of nickel electrode capacity decrease.

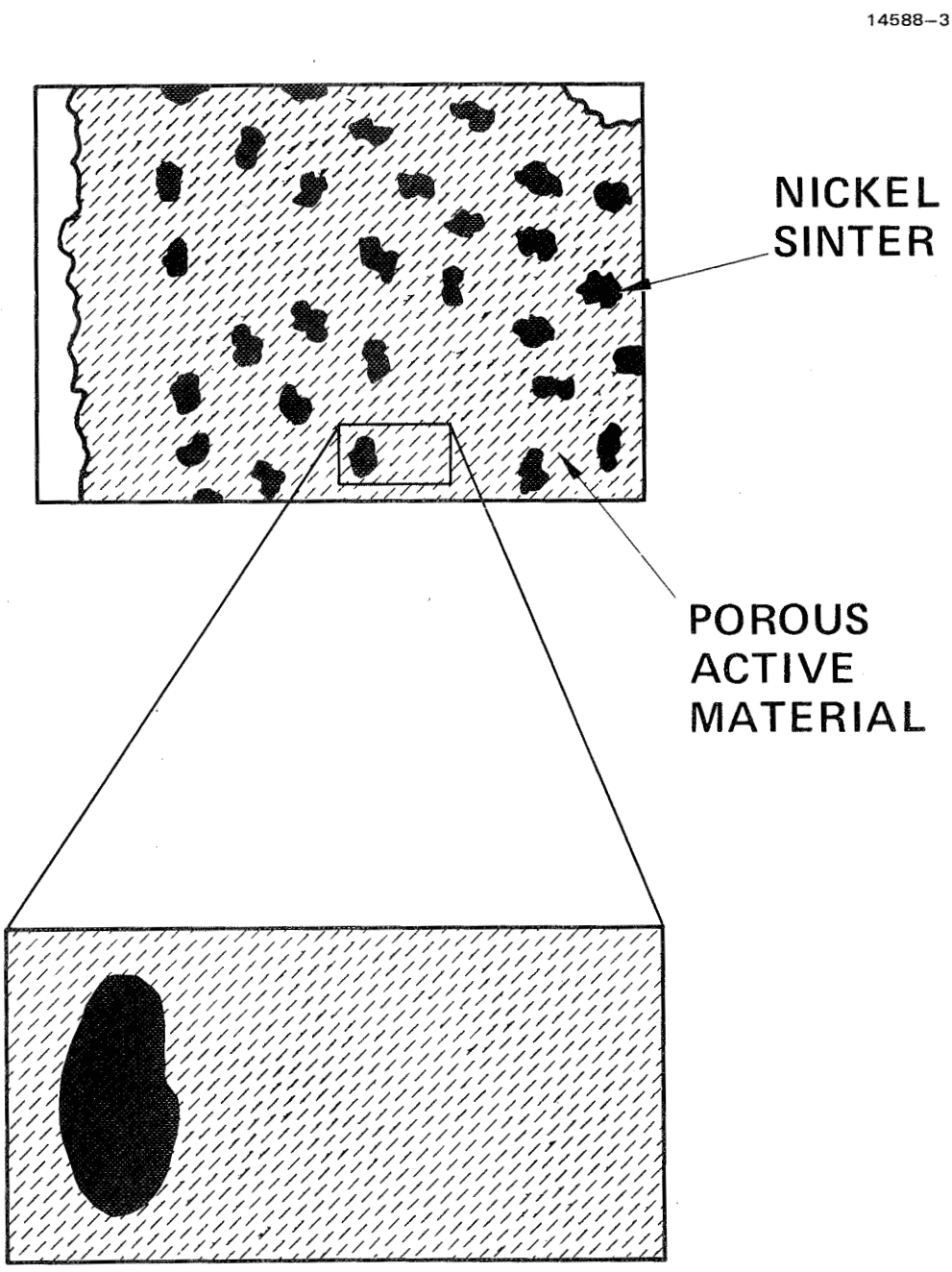

Figure 11. A schematic representation of a microscopic portion of a nickel electrode.

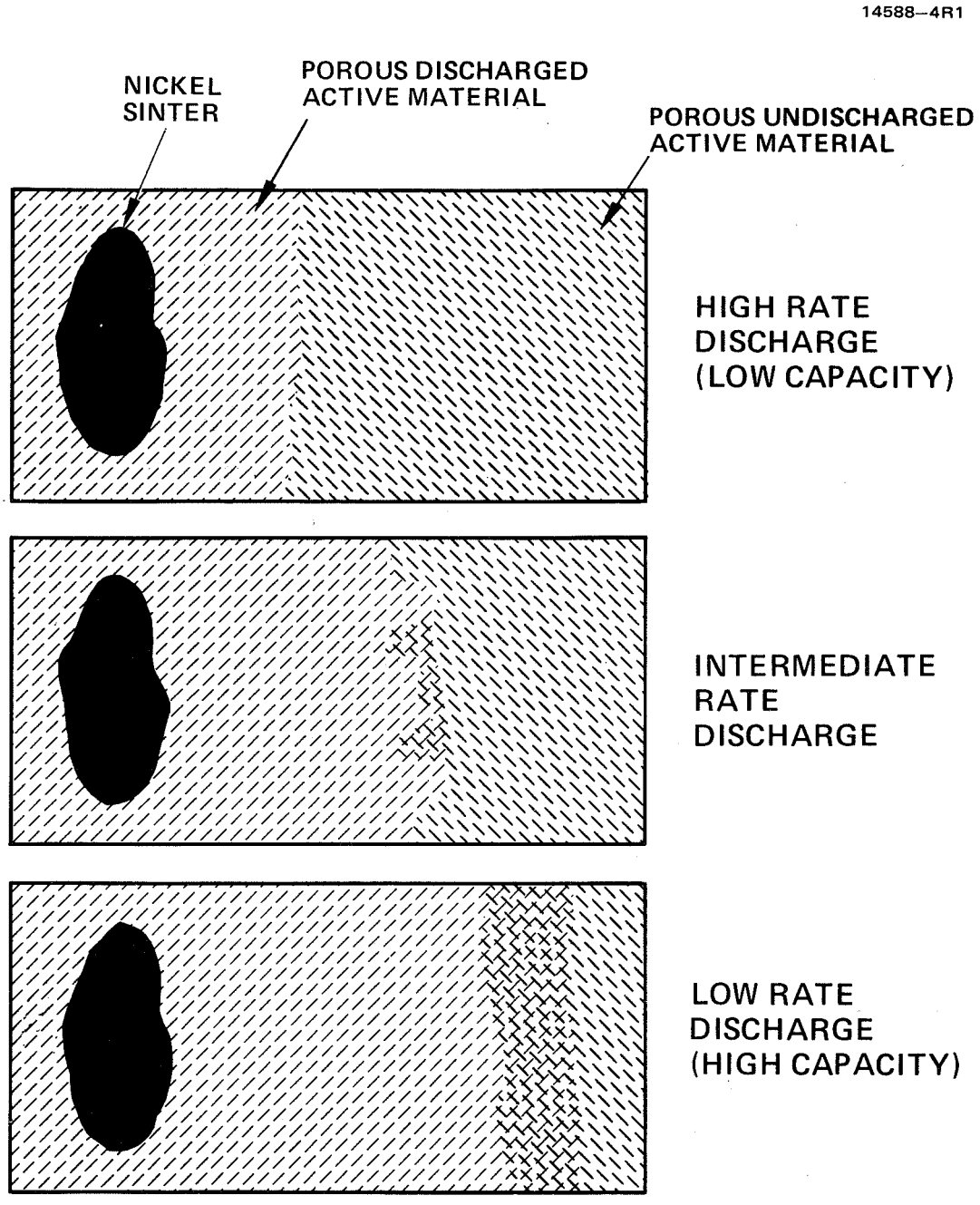

Figure 12. A schematic illustration of discharge rate dependence of electrode capacity.